Frontiers in Bioscience Scholar

Front. Biosci. (Schol Ed) **2022**; 14(4): 27
https://doi.org/10.31083/j.fbs1404027

Original Research

A New Drug-Free Cancer Therapy Using Ultraviolet Pulsed Irradiation. PDT (PhotoDynamic Therapy) to PPT (Pulsed Photon Therapy)

Johbu Itoh[1,*], Yoshiko Itoh[1]

[1]Department of pathology, School of Medicine, Tokai University, 259-1193 Isehara, Japan
*Correspondence: itohj@is.icc.u-tokai.ac.jp (Johbu Itoh)

Academic Editor: Angelo Facchiano
Submitted: 10 June 2022 Revised: 1 August 2022 Accepted: 5 August 2022 Published: 30 September 2022

Abstract

Background: Pulsed ultraviolet (UV) irradiation can be used to generate a broad UV-C spectrum. The pulsing nature of such a spectrum helps increase the damage to cancer cells, leading to their injury and death. In contrast, non-tumor cells repair the damage and survive the same pulsed UV irradiation energy. Herein, we describe the development of a pulsed UV irradiation method for cancer cell dysfunction that irradiates cells with pulsed light by generating tremendous instantaneous UV energy—tens of thousands of times greater than that generated by UV lamps—to cause specific cell injury and dysfunction of cancer cells. **Methods**: A newly developed pulsed ultraviolet irradiation device was used. Features of the device used in this study. This device employs a quartz discharge xenon lamp. Cultured tumor cells and non-tumor cells were irradiated with pulsed light at different irradiation doses, and their reactions were observed using optical, electron, and laser microscopes. **Results**: Cancer cells have more FAS (CD95) receptor domains than non-cancer cells, and pulsed UV irradiation stimulates the production of reactive oxygen species (ROS) and OH, which exceeds the oxidative stress removal function, resulting in cell injury and death. That is, at low UV doses, only cancer cells underwent cell death, whereas non-cancer cells did not. The pulsed UV irradiation technique directly destroys cancer cells and minimizes the number of residual cancer cells while allowing minimum invasion into non-tumor cells, thereby improving their survival. This suggests the possibility of activating the host's local immune response to eliminate residual cancer cells. **Conclusions**: A newly developed pulsed UV radiation system shows potential for use in the development of a drug-free cancer treatment system that selectively kills tumor cells by irradiating them with high-intensity pulsed UV rays over a broad UV-C range of 230–280 nm.

Keywords: pulsed UV irradiation; drug-free pulsed photon therapy; targeted cancer therapy; cancer cell injury; cancer cell death

1. Introduction

Traditionally, the three main cancer therapies include surgery (surgical resection, endoscopic resection, etc.), chemotherapy, and radiation therapy. However, these strategies are not specific to cancer cells and can cause off-target damage to the surrounding normal cells, tissues, and organs. For example, in anticancer drug therapy, cellular injury is observed in normal and cancer cells. While this therapy is based on the fact that normal cells recover more quickly than cancer cells, anticancer drug resistance often develops, rendering them ineffective. In addition, combinatorial therapies comprising multiple anticancer drugs are often administered, which may exhibit increased efficacy but also increases the burden on the patient's body. Meanwhile, surgery requires marginal resection of the normal tissue cells surrounding the cancer, which may result in cancer cells remaining after the surgical intervention. Radiotherapy also damages normal cells and tissues within the irradiated area, which places a heavy burden on the patient. Therefore, developing a specific cancer therapy capable of specifically targeting cancer cells without damaging normal healthy cells and tissues is promising. To this end, near-infrared photoimmunotherapy (NIR-PIT, aka., photoimmunotherapy), using near-infrared light, has attracted attention as a new cancer treatment method [1–3]. Indeed Japan has led the way in NIR-PIT administration, having already demonstrated some success in cancer patients. In fact, the medical community and patients have predicted that photoimmunotherapy will represent the "fifth cancer treatment method", following anticancer agents, surgery, radiation, and cancer immunotherapy.

Photoimmunotherapy is an innovative treatment that can be used to damage and kill cancer cells. As a pretreatment, a drug combining cancer cell-specific antibodies and light-reactive chemicals are administered intravenously, allowing the antibodies to reach the cancer cells in approximately one day [1–3]. When near-infrared light is incident on the affected area, a chemical reaction occurs, and the cancer cells are destroyed. In addition, Kobayashi and Choyke [4] reported further enhancement of NIR-PIT efficacy, designated as SUPR (super-enhanced permeability and retention effects). Under the SUPR effect, drug-based NIR-PIT only kills perivascular antigen-expressing tumor cells, leaving tumor vessels intact early after treatment while also allowing a significant increase in blood vol-

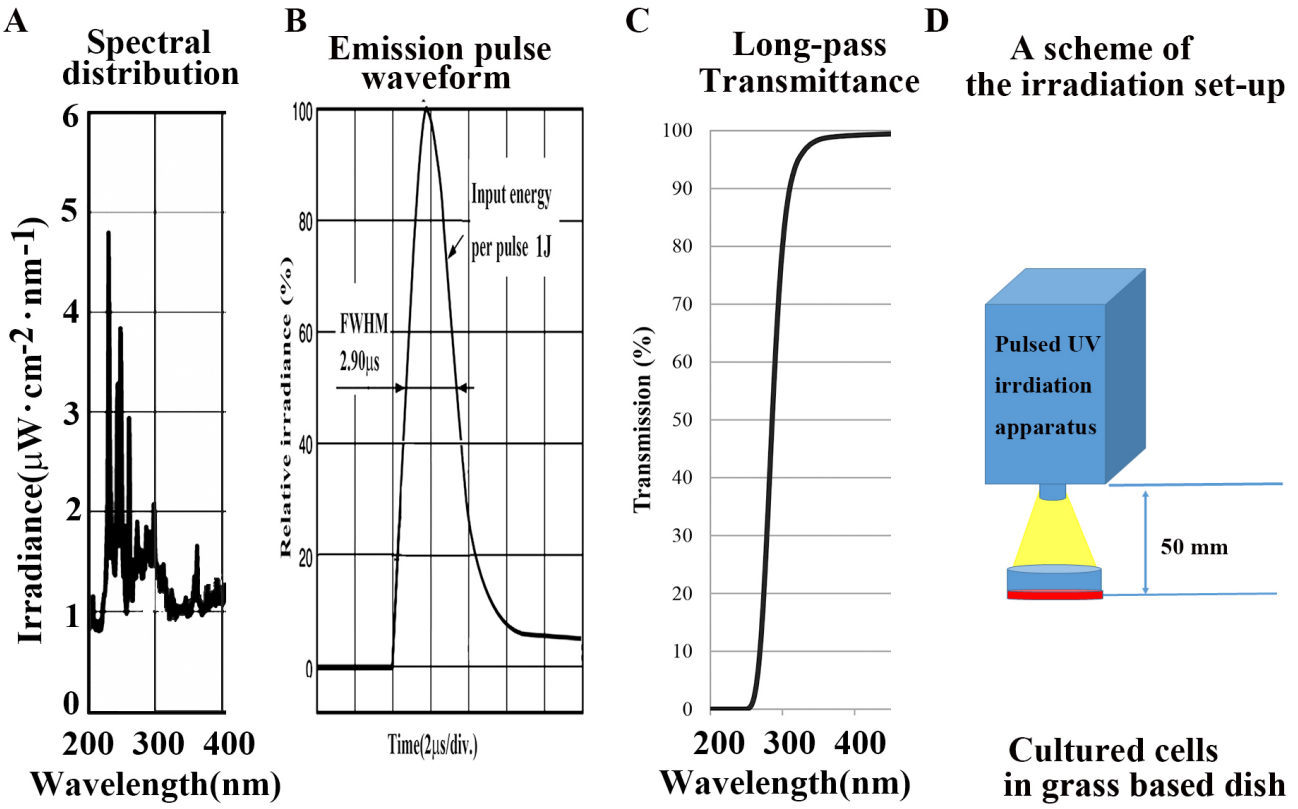

Fig. 1. Characterlizations of equipment used in this article. (A) Spectra in the UV region (200–400 nm). (B) Emission pulse waveform. (C) Internal transmittance curve in a long-pass filter (UV N-WG280; absorption 200–280 nm, Edmund Optics Japan, Japan) in the UV region of a UV pulse flash to be indicated from a xenon flash lamp (S-BP60, Thunderlight Corp. Japan) at a light source. (D) Scheme of the irradiation setup. The total exposure energy was compared at 0, 25, 50, 100, 200, and 500 mJ/cm^2 at a distance of 5 cm.

ume and nanodrug perfusion into the tumor bed within tumor vessels immediately after NIR-PIT. Cellular injury by drug-induced NIR-PIT reportedly occurs in the perivascular layer of tumor cells and is accompanied by marked dilation of tumor vessels in the dilated tumor stroma [4]. Notably, this regimen also requires the administration of a hybrid drug comprising cancer cell-specific antibodies and photoreactive chemicals as pretreatment. Although the mechanism of action is different, similar vasodilatation effects can be obtained with drug-free pulsed UV irradiation methods.

UV rays elicit bactericidal effects [5–8]; low-pressure mercury vapor lamps (UV lamps) have long been used as sterilizing lamps. In recent years, "optical pulse sterilization" using xenon flash lamps has proved to be a novel technique [9–12]. Xenon flash lamps can instantaneously emit light in the 200–300 nm wavelength range, which is considered highly effective for sterilization in the order of microseconds; each of which provides tens of thousands of times more energy than a UV lamp (~65 W). Light pulse sterilization with xenon flash lamps is a method that demonstrates high sterilizing power in an extremely short time (less than one second to several seconds) against bacteria, molds, and spore-forming fungi. Accordingly, this method is beginning to be put into practical use in food preparation, as well as in other fields [9,13,14]. However, its application in selective damage and death of tumor cells by pulsed light using xenon flashlamps or similar devices has not been reported. In this study, we developed a new cancer therapy using specific xenon lamp pulsed irradiation that selectively injures cancer cells and causes cell death without drug injection (drug-free).

2. Materials and Methods

2.1 Pulsed UV Irradiation Apparatus

A newly developed pulsed UV radiation system was used (S-BP60, Thunderlight Corporation, Kanagawa, Japan). The luminescent characteristics of the UV field are shown in Fig. 1A. This apparatus has a quartz discharged xenon lamp with a pulse full-width half-maximum of 0.29 μs and a frequency of 60 Hz. The input energy of the lamp was 1.0 J per pulse, and was 60 J per second at a frequency of 60 Hz. A long-pass filter (UV N-WG280; absorption 200–280 nm, Edmund Optics Japan, Japan) was used to verify the effect of UV-C irradiation on cells. The internal transmittance characteristics of the UV field are shown in Fig. 1C.

2.2 Ultraviolet Luminance Analysis

An FUD-7010J system (FUJIFILM Corporation, Japan) was used for ultraviolet light intensity distribution analysis. This system enables digitization of UV, integrated light intensity values, as well as analysis and storage of the UV light intensity distribution by reading the color development of the UV scale.

The cellular effects of pulsed UV irradiation on tumors were compared with those induced by pulsed UV irradiation at 0, 25, 50, and 100 mJ/cm^2. The cells were continuously cultured after irradiation, and cell viability (dead cells/total cells) was analyzed 4–40 h later using the IMRIS image analysis software 9.0.2 (Bit Plane, Zürich, Switzerland).

2.3 Cell Lines and Growth Conditions

MCF-7 (human breast adenocarcinoma, EACC) and Cos7 (African green monkey cell line producing the T antigen of SV40) were routinely cultured in DMEM (Dulbecco's modified Eagle's medium) high glucose and 10% fetal bovine serum obtained from Gibco (Thermo Fisher Scientific K.K. Japan) in 35 mm diameter glass-based dishes (IWAKI (AGC), Japan) and maintained in a humidified incubator at 37 °C with a 5% CO_2 atmosphere.

2.4 Confocal Laser Scanning Fluorescence Microscopy Imaging

Cultured MCF-7 and Cos7 cells were analyzed with and without fixation in 4% paraformaldehyde (PFA), primarily using ZEISS LSM880 (ZEISS, Germany). Fixed cells were covered with a 10% glycerol solution to prevent drying, while living cells were observed under culture. Cells were observed using Plan-Apochromat lenses (10×, numerical aperture = 0.45, M27, ZEISS) and C-Apochromat lenses (63× numerical aperture = 1.2 Water). Spectral unmixing of the obtained images was performed using ZEN imaging software (Carl Zeiss Microscopy, Jena, Germany). The spectrum from propidium iodide (PI; maximum peak emission fluorescence wavelength: 580 nm) was detected in the cells from dead cell nuclear and mitochondrial DNA. Hence, PI was used to detect cell death. That is, due to the presence of a solid membrane structure in living cells, PI does not permeate the cell, and consequently does not show red staining. Conversely, a dead cell with a broken membrane structure allows PI to infiltrate the cell and react with nuclear DNA and mitochondrial DNA, consequently staining red.

Pulsed UVC-irradiated, non-irradiated, and UV-C-irradiated cells were also compared. Cell viability (dead cells/total live and dead cells) was analyzed 4–40 h after irradiation using the IMRIS (Ver 9.0.2) image analysis software (Bitplane AG, Switzerland). Additionally, some 12- and 24-h time-lapse observations were performed.

2.5 Transmission Electron Microscopy (TEM)

The cells were fixed in glutaraldehyde solution for 1–2 h at 4 °C. Post-fixation, cells were incubated in 1% osmium tetroxide solution for 2 h at 4 °C. The cells were then embedded in an epoxy resin for 6 h. A plastic embedding plate (or gelatin capsule) with fresh epoxy resin was filled, and the tissue was placed in it and allowed to polymerize in an incubator at 60 °C for three days. Ultrathin sections were observed under an electron microscope JEM-1400 (JEOL, Japan).

2.6 Scanning Electron Microscopy (SEM)

Briefly, the cells were fixed in 4% paraformaldehyde dissolved in 0.01 M phosphate-buffered saline pH 7.4 (PBS). After fixation, cells were processed in a conventional manner using a JSM-6510LV electron microscope (JEOL, Japan).

2.7 Immunocytochemical and Histochemical Analysis

2.7.1 CD95

To reveal the immunocytochemical localization of CD95, CD95 (FAS) antibody, anti-human, PE, REAfinity™ (Miltenyi Biotec, Germany) were used. A total of 2×10^5 cultured cells were added to each 35 mm diameter glass-based dish. The antibody dilution was 1:50 (PBS/EDTA/BSA buffer) in a final volume of 100 μL. The culture medium was removed, and cells were washed three times with PBS for 5 min each, fixed with 4% PFA (26126-25, Nacalai Tesque) in 0.1 M PBS at RT for 20 min, and washed three times with PBS for 5 min each. They were then incubated with PBS containing 1:50 diluted CD95-PE antibody for 10 min in the dark in a refrigerator (2–8 °C) and washed three times with PBS for 5 min each [15].

2.7.2 Annexin V

For the cytochemical detection of Annexin V, a multiparameter apoptosis assay kit (Cayman Chemical, MI, USA) was used. Using Annexin V-FITC reagent (maximum peak emission fluorescence wavelength: 517 nm) phosphatidylserine (PS) is redistributed to the external plasma membrane of apoptotic cells. Annexin V staining can result in morphological changes in the cells or even their release from the culture surface.

2.7.3 Tetramethylrhodamine Ethyl Ester (TMRE) Dye

To determine mitochondrial membrane potential, the TMRE dye (maximal fluorescence wavelength: 595 nm) in the Multi-Parameter Apoptosis Assay Kit (Cayman Chemical, MI, USA) was used. TMRE is a cell-permeant, cationic, red-orange fluorescent dye that is readily sequestered by the active mitochondria. The membrane potential was thus preserved.

Briefly, Annexin V and TMRE staining was performed as follows. Cultured cells (2×10^5) were treated as necessary in a CO_2 incubator at 37 °C, with each sample

in duplicate or triplicate. Cells were <80% confluent at the time of staining. The culture medium (DMEM) from each 35 mm diameter glass-based dish, as well as the cell layer, were not disturbed. Subsequently, 250 μL of the staining solution was added to each dish. The cells were incubated at room temperature in the dark for 15 min. The staining solution was carefully removed, and 500 μL of PBS (pH 7.4) was added. To the PBS, 2.0 mL of DMEM and 2 μL PI solution were added per dish.

2.7.4 Oxidative Stress Analysis

Oxidative stress results from an imbalance between ROS production and the ability of cells to scavenge ROS. ROS plays an important role in the progression of several diseases, including inflammation, atherosclerosis, aging, and age-related degenerative disorders [16]. To detect oxidative stress in cells, CellROX™ Deep Red Reagent (Molecular Probes; Thermo Fisher Scientific K.K., Japan) was used. CellROX™ Deep Red Reagent is a novel fluorogenic probe for measuring cellular oxidative stress in both live and fixed cell imaging, with an emission maximum at 665 nm. The cell-permeant dye is non-fluorescent in a reduced state and exhibits bright fluorescence upon oxidation by reactive oxygen species (ROS).

2.7.5 Caspase-3/7 Activity Analysis

To detect caspase-3/7 activity in the cells, CellEvent™ Caspase-3/7 Green Detection Reagent (Invitrogen, Thermo Fisher Scientific K.K. Japan) was used (maximum peak emission fluorescence wavelength: 530 nm). CellEvent™ Caspase-3/7 Green Detection Reagent is a novel fluorogenic substrate for activated caspases 3 and 7. The reagent consists of a four-amino acid peptide (DEVD) conjugated to a nucleic acid-binding dye. This cell-permeant substrate is intrinsically non-fluorescent because the DEVD peptide inhibits the ability of the dye to bind to DNA. Following activation of caspase-3 or caspase-7 in cytotoxic cells, the DEVD peptide is cleaved, enabling the dye to bind to DNA and produce a bright, fluorogenic response with an emission maximum of 530 nm.

2.7.6 Reactive Oxygen Species (ROS) Detection

To determine the ROS activity in the cells, 3,3-(p-hydroxyphenyl) fluorescein (HPF) was used as an indicator of ROS (Invitrogen, Thermo Fisher Scientific K.K. Japan) with a maximum peak emission fluorescence wavelength: 515 nm. HPF exhibits limited non-selective reactivity and relatively high resistance to light-induced oxidation. The new fluorescein derivatives are non-fluorescent until they react with the hydroxyl radical or peroxynitrite anion. ROS indicators can be used to selectively detect hypochlorite anions.

Briefly, cultured cells (2×10^5) were prepared in a 35 mm diameter glass-based dish. The dimethylformamide (DMF) stock solution was diluted to a suitable buffer concentration of 1–10 μM. The cells were incubated with the diluted HPF for 60 min at 37 °C. Cells were then washed to remove the excess probe, and the medium was replaced with fresh DMEM.

2.7.7 Hydroxyl Radical (•OH) Detection

To detect intracellular hydroxyl radicals (•OH), the Cell Meter™ Mitochondrial Hydroxyl Radical Detection Kit *Red Fluorescence* MitoROS™ OH580 (AAT Bioquest, California. USA) was used (maximum emission fluorescence wavelength: 598 nm). Detection of intracellular •OH is of utmost importance for understanding proper cellular redox regulation, and the impact of its dysregulation on various pathologies. •OH is an ROS that is highly reactive with other molecules to achieve stability. Hence, •OH is considered a harmful by-product of oxidative metabolism and can cause molecular damage in living systems. It shows an average lifetime of 10–9 ns and can react with nearly every biomolecule, such as nuclear DNA, mitochondrial DNA, proteins, and membrane lipids. This kit is optimized for detecting •OH in the mitochondria. MitoROS™ OH580 is a live cell-permeant probe that can rapidly and selectively target •OH in live cells after only 1 h of incubation. Red fluorescence is generated when it reacts with •OH.

In brief, the medium was removed, and 200 μL/dish of MitoROS™ OH580 working solution was added to each cell dish and further incubated at 37 °C for 60 min. To induce •OH, cells with the test compound were treated with pulsed UV radiation at 37 °C in PBS, shielded from light. After washing 2–3 times with PBS, 100 μL of assay buffer and 2 mL of DMEM were added to each dish.

3. Results

3.1 Pulsed UV Irradiation in Tumor and Non-Tumor Cells

The integrated irradiance per unit area [J/cm^2] is a function of the output [J/h] and irradiation frequency [time] of the light source of the UV pulse flash in one irradiation. The integrated output [J] is the total value and the irradiated area [cm^2] of the UV pulse flash. Furthermore, when the light source is regarded as a point light source, the integrated irradiation output per unit area of the UV pulse flash [J/cm^2] is inversely proportional to the square of the distance from the light source.

As shown in Fig. 2, when a xenon flash lamp (S-BP60, Thunderlight Corp.) was used as the light source for pulsed UV irradiation and the distance between the xenon flash lamp and the irradiated area was 5 cm, UV irradiation at 25 mJ/cm^2 or higher could damage and kill more than 90% of tumor cells (MCF-7). Whereas UV irradiation of 50 mJ/cm^2 or more could damage and kill most tumor cells, resulting in a tumor cell survival rate of 5% or less after 24 h of irradiation. Moreover, UV irradiation at 100 mJ/cm^2 or more almost completely eliminated the tumor cells. Under the above conditions, UV irradiation of 100 mJ/cm^2 or less induced only negligible effects on non-tumor cells with

Table 1. Tumor cell lines for which xenon pulse irradiation has shown *in vitro* efficacy, cell injury, and cell death.

Tumor cells			Non-tumor cells		
Human	Type of cell	Cell name	Human	Cell type	Cell name
1	Human breast cancer cell line	MCF7	1	Human mammary epithelial cell	HMEC
2	Human breast cancer cell line	BT474	2	Leukocytes	Leukocytes
3	Human Cervical Cancer cell line	HeLa	3	plasma	plasma
4	Human leukemia cell line	MOLT/S	Monkey		
5	Human leukemia cell line	MOLT/TMQ 200 (Trimetrexate (TMQ) anti cancer drag resistance 200 times)	1	African green monkey cell	Cos7
6	Human leukemia cell line	K562/S1	Dog		
7	Human leukemia cell line	K562/S2	1	Canis normal kidney	MDCK
8	Human leukemia cell line	K562/ARA-C (Cytarabine anti cancer drag resistance)	Mouse		
9	Human fibrosarcoma cell line	HT-1080	1	Mouse fetal fibroblast	NIH3T3
10	Human prostate cancer cell lines	DU145			
11	Human prostate cancer cell lines	PC3			
12	Malignant cell lines of human choriocarcinoma	BeWo			
13	Human renal cancer cell line	ACHN			
14	Human renal carcinoma cell line	Caki1			
Mouse					
1	mouse lymphoma	EL-4			
2	mouse lymphoma	A20			
3	mouse lymphoma	RL male 1			
4	mouse lymphoma	B16			

a survival rate after 24 h irradiation of ~100%. Therefore, when this method was applied to tumor cells, such as human breast cancer cells, the preferred range of the exposure dose of pulsed UV irradiation under the above conditions was 25–100 mJ/cm^2 UV light that could damage and kill most of the tumor cells and would allow almost complete survival of non-tumor cells.

As shown in Table 1, the tumor cells that showed efficacy in this method included cancer (malignant tumors of epithelial tissue origin), sarcoma (malignant tumors of non-epithelial tissue origin), leukemia, malignant lymphoma, benign tumor cells, and cell lines. In contrast, non-tumor cells are intact cells other than tumor cells. Hence, this method can be applied to sites where tumor cells and non-tumor cells are mixed.

Additionally, transmittance observations and spectral analysis of PI fluorescence was performed using LSM880 (Figs. 2,3). Atrophy was observed in all cells used in the experiments; however, irradiation at 25 mJ/cm^2 resulted in pronounced cell atrophy, with morphology that could be attributed to changes in the cell surface membrane structure. Similarly, cell atrophy and changes in the cell membrane structure were observed by transmission and scanning electron microscopy (Figs. 2C,3B). Regarding the cell viability observed after 24 h of irradiation, the viability of non-tumor cells remained nearly 100% at 100 mJ/cm^2 irradiation. Conversely, the survival rate of tumor cells decreased from approximately 10% at 25 mJ/cm^2 UV irradiation to 4% at 50 mJ/cm^2 irradiation and nearly 0% at 100 mJ/cm^2 irradiation (Fig. 2D). That is, irradiation with a 100 mJ/cm^2 UV pulse flash at a distance of 5 cm from the light source resulted in ~100% survival of non-tumor cells, and almost completely eliminated tumor cells. In addition, morphological observations revealed that irradiation with 500 mJ/cm^2 also altered the membrane structure of non-tumor cells, with some cell death observed (data not shown). In contrast, no significant difference in viability was observed between tumor cells and non-tumor cells when the UV-C of UV pulsed light was excluded by a long-pass filter (cut below 280 nm) (Fig. 3C).

Pulsed UV (including UVC) irradiation killed tumor cells at 100 mJ/cm^2, whereas nearly 100% of non-tumor cells survived. Morphological observations revealed that dead cells exhibited cell membrane injury, disruption, cytoplasmic lysis, disruption of intracellular organelle membranes, and some nuclear enrichment. Based on these results, the hypothesis shown in Fig. 4 was formulated, and experiments were conducted to test it.

3.2 Immunocytochemical and Histochemical Analysis

3.2.1 CD95 (FAS)

The death receptor (CD-95) is highly expressed on tumor cell membranes, and its localization was observed by immunocytochemical assay (Fig. 5) [15,17,18]. In tu-

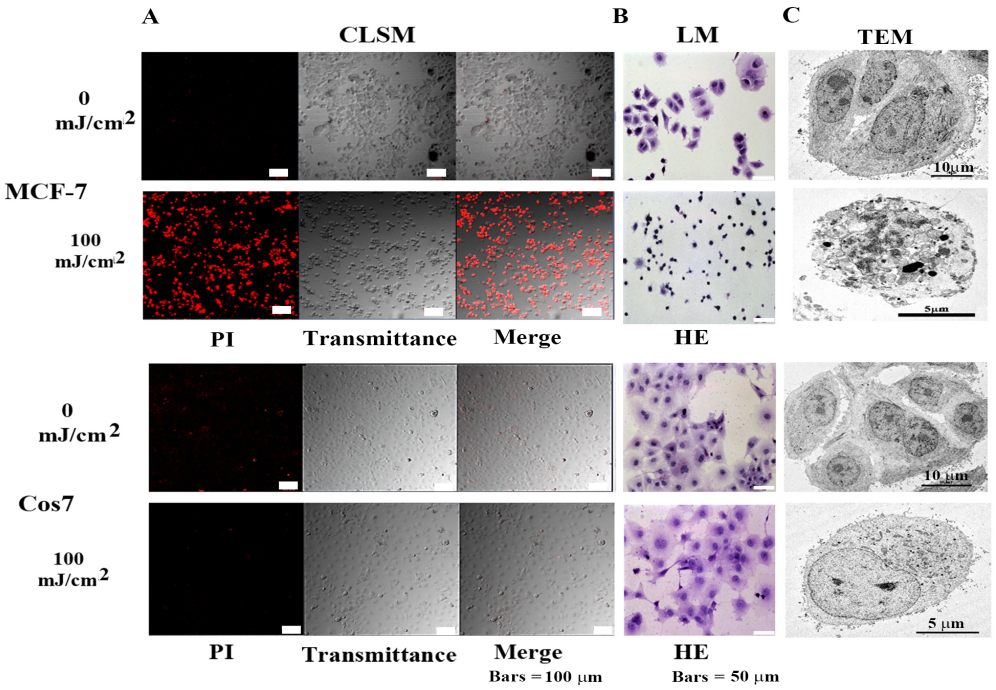

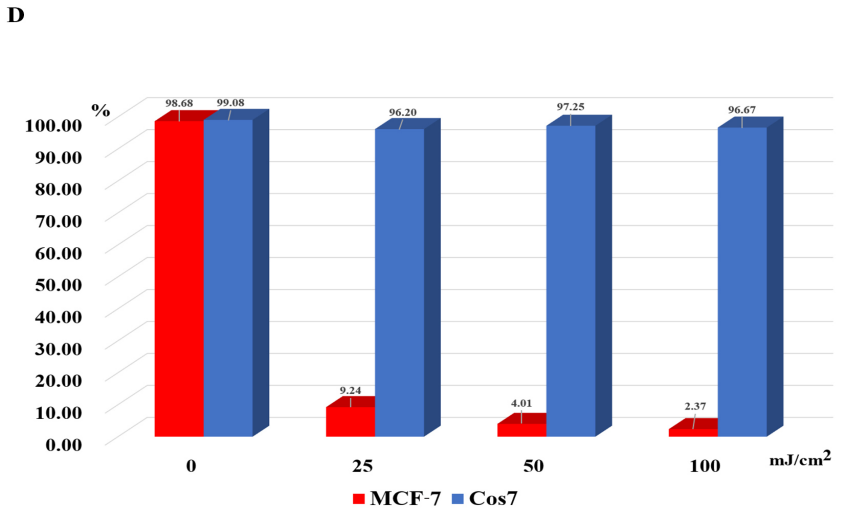

Fig. 2. Microscopic observation of tumor cells (MCF-7) and non-tumor cells (Cos7) 24 h after irradiation. (A) Confocal laser scanning microscopy images. In MCF7 tumor cells, most in the control group survived, while most tumor cells in the 100 mJ/cm^2 UV irradiation group died. In non-tumor Cos7 cells, nearly all cells survived in the control and treatment groups. Note: dead cells appear red. (B) Light microscopy images. In MCF7 tumor cells, nuclei and cytoplasm were clearly observed in the control group, while under 100 mJ/cm^2 UV irradiation, the cytoplasm was lost, and only enriched nuclei were observed. In contrast, in non-tumor cells (Cos7), no change in cell morphology was observed between the two groups. (C) Transmission electron microscopy images. In MCF7 tumor cells, nuclei and subcellular organelles were clearly visible for the control cells. However, in the 100 mJ/cm^2 UV irradiation, the subcellular organelles, and nuclear structure were unclear. Additionally, cell membrane damage, cellular content leakage, cytoplasm shrinkage, and blurred/indistinct cell membrane were observed. In non-tumor cells (Cos7), no change in cell morphology was observed in either group. (D) Cell viability observed 24 h after irradiation with a UV pulse flash (irradiation energy: 0, 25, 50, 100 mJ/cm^2). Cell viability = dead cell count/all cells count × 100 (%). In tumor cells, cell death increased in proportion to the irradiation dose, while no change was observed in non-tumor cells.

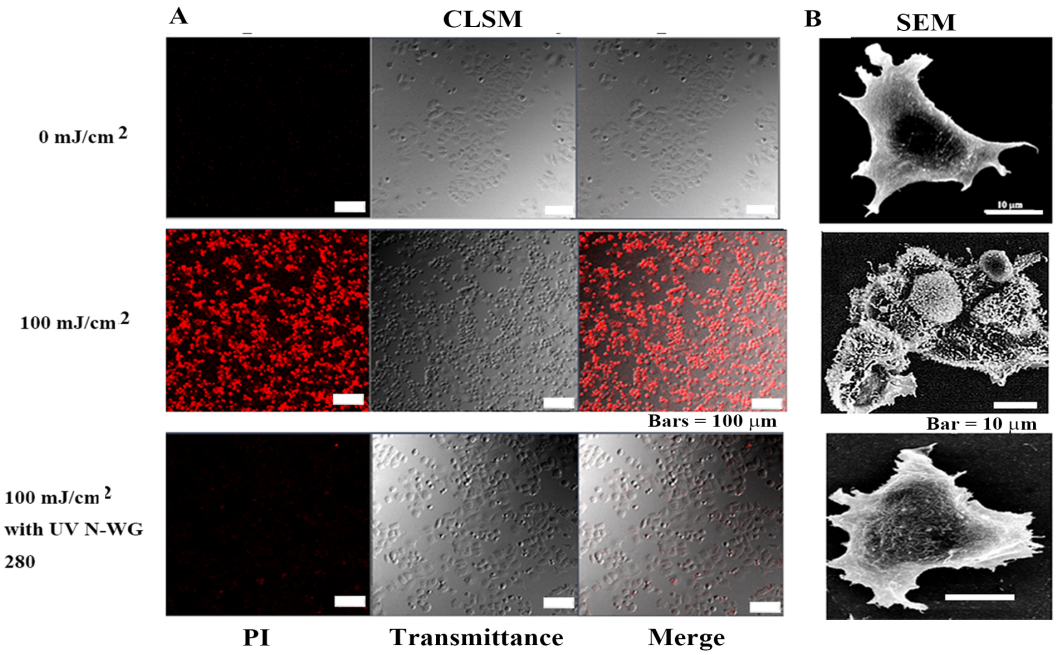

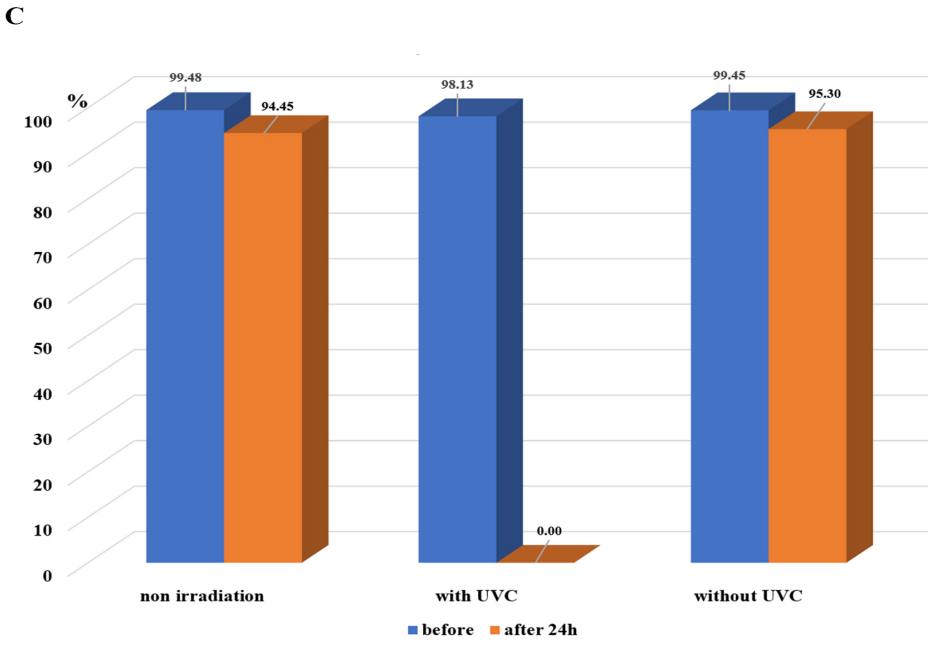

Fig. 3. Selective tumor cell (MCF-7) injury and death is determined by the presence or absence of UV pulse irradiation. (A) Images of MCF-7 tumor cells observed by confocal laser scanning microscopy after 24 h of irradiation. The tumor cells in the control group survived, while nearly all treated tumor cells died. Tumor cells survived following irradiation exposure after removing UV-C with a long-pass filter UV N-WG280. (B) Scanning electron microscopy images of MCF7 cells after 24 h of irradiation. In the control group, the nucleus, and subcellular organelles were clearly observed; in the 100 mJ/cm^2 UV irradiation group, significant membrane disruption, cell atrophy, cellular content leakage, cytoplasm shrinkage, and blurred/indistinct cell membranes were observed. Cell membranes and smooth surfaces, similar to those of control cells, were observed following the removal of UV-C. (C) Cell viability 24 h after irradiation with a UV pulse flash from which UV-C was removed (irradiation energy: 0, 100 mJ/cm^2). Cell viability = dead cells/all cells × 100 (%). In MCF7 cells treated with 100 mJ/cm^2 irradiation, most cells died, while no change was observed in UVC-cut cells following irradiation.

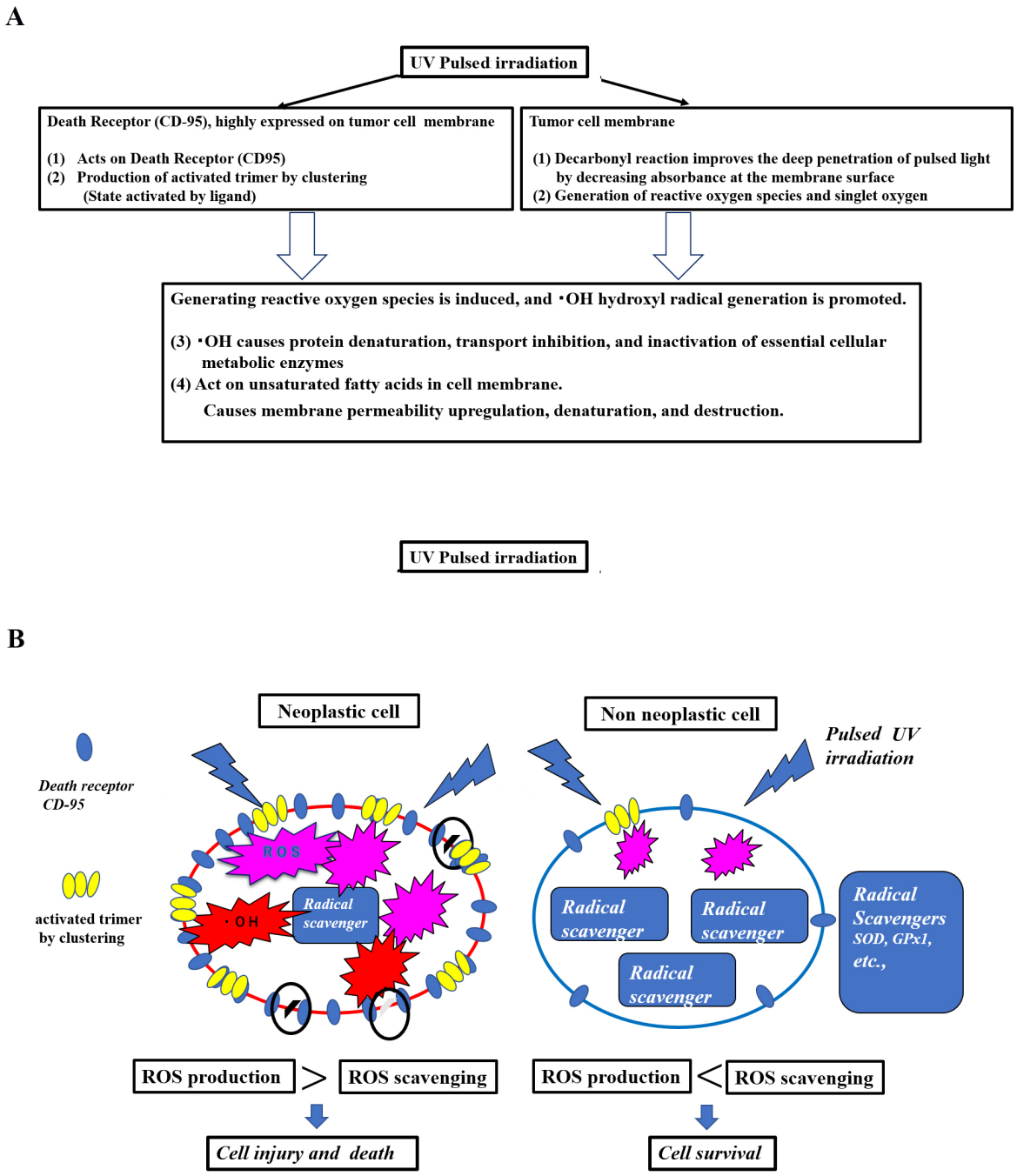

Fig. 4. Hypothesis of a mechanism of selective tumor cell injury/killing in pulsed light irradiation. (A) Hypothesis: Cellular injury and death due to pulsed UV irradiation membrane disruption. (B) Hypothesis: Cellular injury and death due to scheduled UV membrane disruption in neoplastic cells vs. non-neoplastic cells. This hypothesis involves selective tumor cell death by pulsed UV irradiation. Functional differences exist between tumor and non-tumor cells. Death receptors, such as CD95, are highly expressed by tumor cells, while being lowly expressed by non-tumor cells. Additionally, radical scavenging is low in tumor cells and high in non-tumor cells. Pulsed UV irradiation directly activates death receptors, such as CD95, thereby inducing receptor trimerization and clustering, primarily in tumor cells. It then induces the production of ROS and further production of •OH radicals. As tumor cells have a lower radical scavenging function, the production of ROS and •OH radicals occurs in a chain reaction, causing membrane destruction of subcellular organelles. Conversely, non-tumor cells express fewer death receptors and have a higher radical scavenging function; therefore, the removal of ROS and •OH radicals is prioritized, and the cells typically survive.

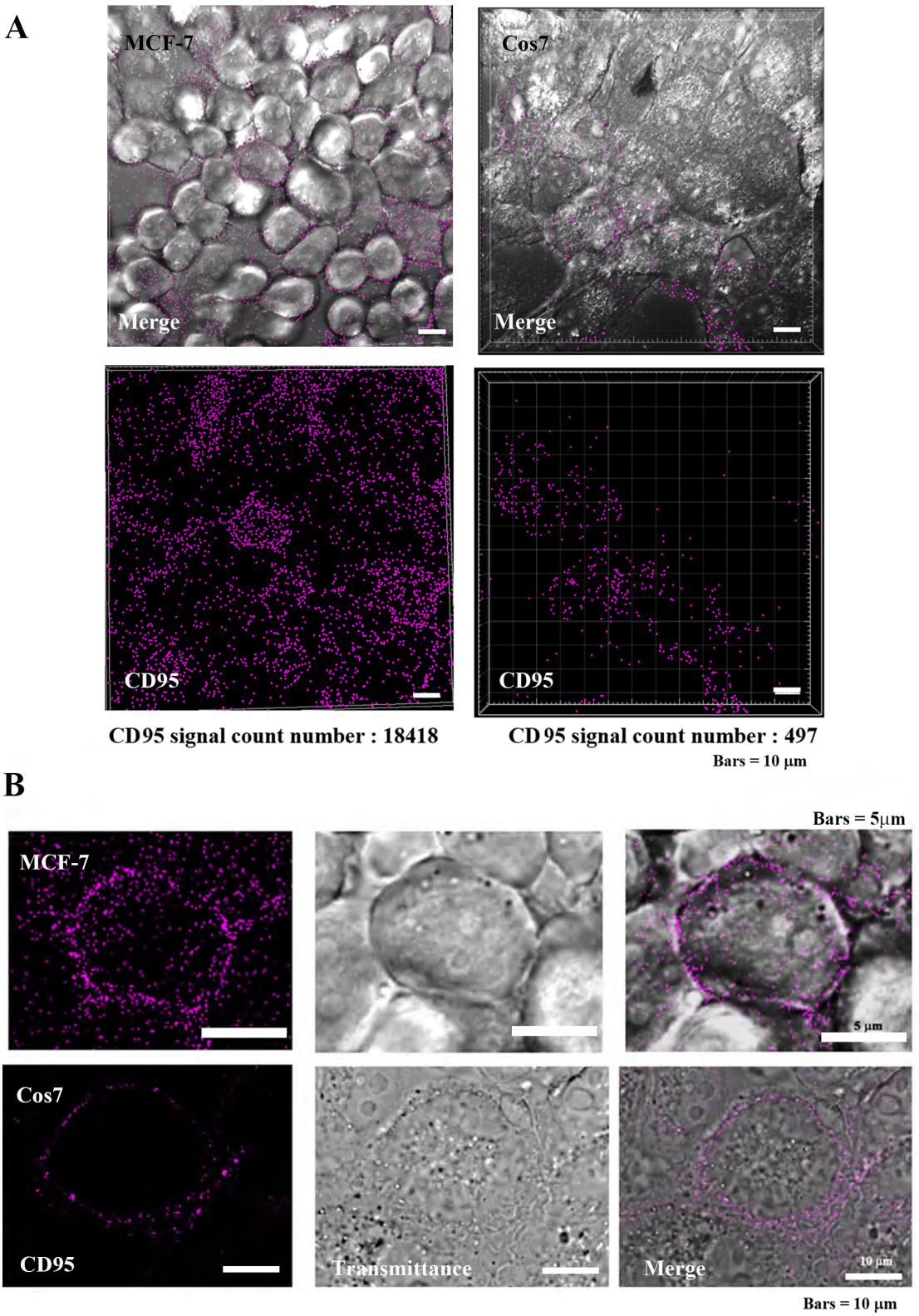

Fig. 5. Localization of CD95 in tumor cells (MCF-7) and non-tumor cells (Cos7). (A) Confocal laser scanning microscopy (CLSM) images (low power magnification, Bars = 10 μm) of MCF-7 and Cos7 cells. (B) CLSM images (high power magnification) of MCF-7 and Cos7 cells. Tumor cells contained a large number of CD95-positive signals on the surface of the plasma membrane, while less fluorescence was observed on the surface of non-tumor cells.

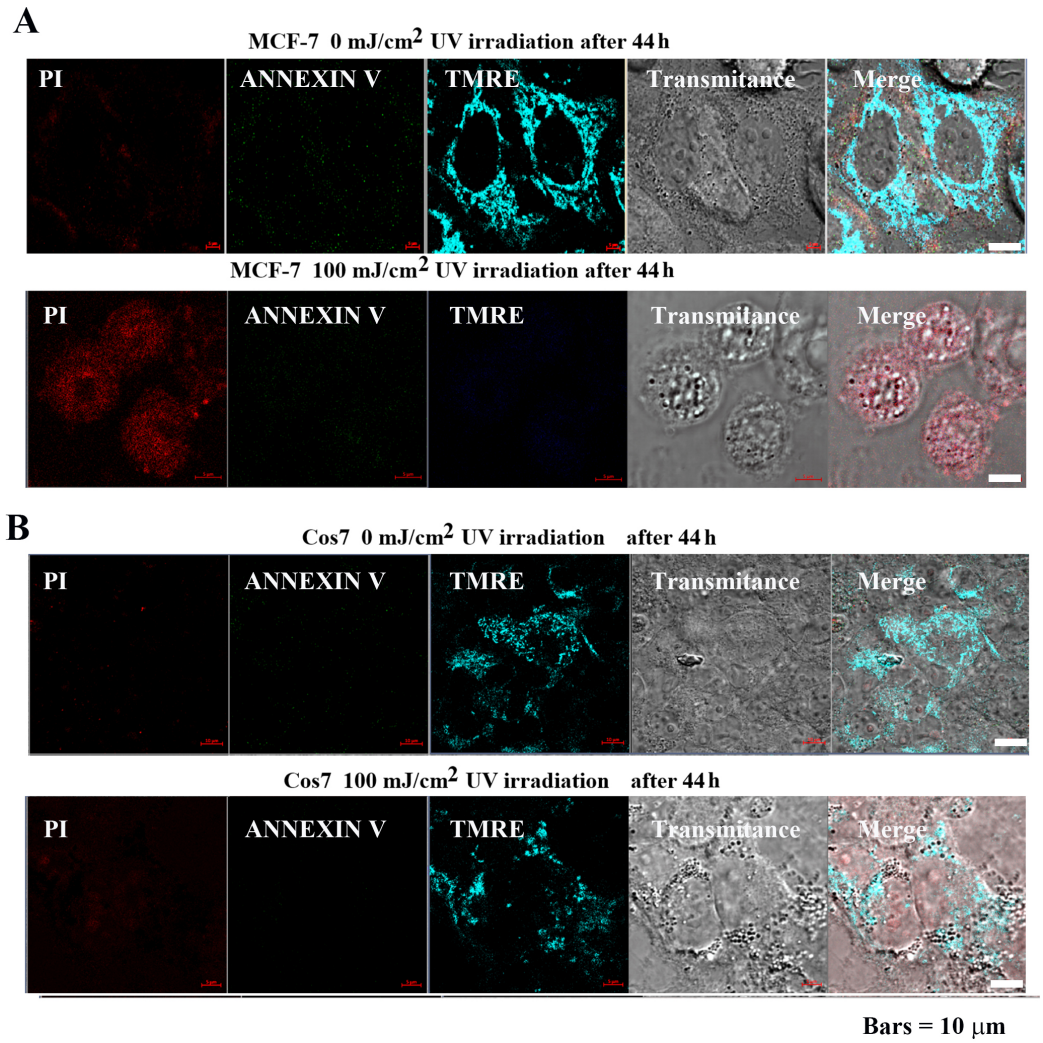

Fig. 6. Impact of pulsed UV irradiation on MCF-7 and Cos7 apoptosis and mitochondrial membrane potential. (A) In MCF-7 cells, the control group exhibited low PI, Annexin V signal intensity, and the tetramethylrhodamine, ethyl ester (TMRE) signal was highly localized in the mitochondria. In contrast, the PI signal intensity increased after 100 mJ/cm^2 irradiation, and Annexin V signal intensity was negligible compared to the controls; TMRE signal intensity disappeared, indicating decreased mitochondrial membrane potential. (B) Cos7 0 mJ/cm^2 control and 100 mJ/cm^2 irradiation images showed low PI and annexin V signal intensity, while TMRE signal intensity was highly localized to the mitochondria. The mitochondrial membrane potential appeared normal.

mor cells MCF7, CD95 was found to be highly localized on the plasma membrane, while in non-tumor Cos7 cells, CD95 was observed at low levels. The IMARIS analysis of positive counts in the same field of view showed MCF7:17418 and Cos7:497 positive grain, indicating that CD95 was approximately 37 times more localized in tumor cells (Fig. 5A). At the individual cell level, the localization of CD95 was clearly greater in tumor cells than in non-tumor cells (Fig. 5B).

3.2.2 Annexin V

Each cell was irradiated with a UV pulse flash at a predetermined irradiation dose, as described above, and the effect on early apoptosis (DNA damage) was examined [19,20]. Using annexin V as a marker, early apoptosis was analyzed by confocal laser scanning microscopy (CLSM) in a similar manner to that of cell viability. In early apoptosis, phosphatidylserine (PS) is expressed on the outer layer of the cell membrane and binds to annexin V, which has a high affinity for PS. Annexin V is a 35–36 kDa protein that binds to phospholipids in a Ca^{2+}-dependent manner, and when PS is expressed on the outer layer of the plasma membrane, the normal plasma membrane structure is lost, and DNA fragmentation and chromatin aggregation are initiated. Based on this principle, early-stage apoptotic cells can be identified by detecting their binding to annexin V [21].

MCF-7 and Cos7 were irradiated with 0 and 100 mJ/cm^2 UV, and CLSM analysis was performed 44 h after irradiation (Fig. 6). Annexin signals were scarcely de-

tected after 0 and 100 mJ/cm^2 UV irradiation in both MCF-7 and Cos7 cells, suggesting that apoptosis is not involved in the mechanism of action underlying the action induced by xenon lamp pulsed irradiation.

3.2.3 Tetramethylrhodamine Ethyl Ester (TMRE) Dye

Mitochondrial membrane potential was analyzed using TMRE to confirm the effect of pulsed UV irradiation on mitochondria. TMRE is a cationic fluorophore of the ethyl ester of rhodamine. Owing to the lipophilic structure of the fluorescent dye, it easily penetrates lipid bilayers, albeit at a slow rate. In mitochondria with membrane potential, it accumulates at high concentrations up to the saturation level and emits red-orange fluorescence. However, when mitochondria lose their membrane potential due to apoptosis or metabolic stress, the fluorescent dye diffuses throughout the cell, and the fluorescence intensity decreases markedly [22].

In MCF-7 cells (Fig. 6A), TMRE signal intensity was high following 0 mJ/cm^2 UV irradiation, with large nuclei, abundant mitochondria, and subcellular organelles observed. Conversely, at 100 mJ/cm^2 UV irradiation, TMRE signal intensity disappeared, indicating decreased mitochondrial membrane potential.

Cell morphology, atrophy, cytoplasmic lysis, disruption of the cell membrane, and destruction of subcellular organelles were observed. In contrast, in Cos7 (Fig. 6B), TMER fluorescence intensity remained high at both 0 mJ/cm^2 and 100 mJ/cm^2, whereas PI fluorescence intensity remained low, indicating that the cells were alive. Cell morphology showed large nuclei, abundant mitochondria, and subcellular granules. Together with the Annexin V results, these findings confirm that the observed cancer cell killing effect elicited by xenon lamp pulsed irradiation is not caused by apoptosis (Fig. 6).

3.2.4 Oxidative Stress (OS)

The CellROX™ Deep Red Reagent was used to confirm the response of tumor cells (MCF-7) and non-tumor cells (Cos7) to oxidative stress (OS) induced by pulsed UV irradiation. In MCF-7 cells, PI and OS signal intensities were extremely low, and cell morphology was normal after 0 mJ/cm^2 UV irradiation (Fig. 7-1A). However, following 100 mJ/cm^2 UV irradiation, the PI and OS signal intensities increased in the mitochondrial region. Moreover, cell morphology showed cell atrophy, cytoplasmic lysis, and loss of cytoplasm, as well as some bare nuclei (Fig. 7-1B).

Additionally, following 100 mJ/cm^2 UV irradiation of MCF-7 cells for 4 h PI was observed throughout the cytoplasm, whereas OS was strongly expressed in the region where the mitochondria were suspected to be present (Fig. 7-1C). The cell morphology comprised cytoplasmic atrophy and indistinct cell membrane borders, while cytoplasmic lysis and intracellular organelles were also observed.

In Cos7 cells, PI and OS fluorescence intensities remained weak at both 0 mJ/cm^2 (Fig. 7-2A) and 100 mJ/cm^2 (Fig. 7-2B), indicating that the cells were alive. Moreover, cell morphology exhibited large nuclei, abundant mitochondria, and subcellular organelles.

3.2.5 Caspase-3/7 Activity

Time-lapse observation of PI and Caspase-3/7 activity detection was performed for 10 h after irradiating MCF-7 with 100 mJ/cm^2 UV. Caspase-3/7 activity began to increase 2.5 h after irradiation; after 4 h, both PI and caspase-3/7 activity had increased; and after 7 h, some cells were destroyed (Fig. 8A).

In the case of 100 mJ/cm^2 UV irradiation, caspase-3/7 activity increased 30 min after irradiation, reached its highest value at 130 min, and subsequently decreased. In contrast, the PI signal remained unchanged until 60 min, after which it increased and then declined rapidly. Following irradiation, mitochondrial caspase 3/7 activity increased, followed by a 120 min delay in PI activity; at 270 min, both signals were antagonistic, followed by a transient increase at 375 min, at which point the cells appeared to have been destroyed. At 30 min after irradiation, only an increase in caspase activity was observed; however, at 150 min, an increase in the fluorescence intensity of both caspase and PI was observed. At 600 min, both the fluorescence intensities decreased sharply, suggesting that the cells were destroyed. However, no change was observed in the 0 mJ/cm^2-irradiated area after either irradiation. Conversely, at 0 mJ/cm^2, neither PI nor caspase 3/7 activity exhibited initial changes. Hence, given that pulsed UV irradiation increased caspase 3/7 activity in tumor cells, cells are believed to be killed by a mechanism of action other than apoptosis.

3.2.6 Reactive Oxygen Species (ROS)

To determine the ROS activity in the cells, HPF—an indicator of high ROS levels—was used. After 40 h at 0 mJ/cm^2, neither PI nor HPF fluorescence signals were detected in MCF-7 cells (Fig. 9-1A). However, after 100 mJ/cm^2 irradiation, both PI and HPF fluorescence signals were highly detected in the cytoplasm (Fig. 9-1B). More specifically, the PI fluorescent signal was strong, whereas that of HPF was strong and diffused throughout the cytoplasm (Fig. 9-1C). Furthermore, cell morphology was unclear, with some cytoplasmic outflow and intracellular granules. However, as the time of irradiation exceeded 40 h, all MCF-7 cells were found to be dead.

Following 0 mJ/cm^2 (Fig. 9-2A) and 100 mJ/cm^2 (Fig. 9-2B) UV irradiation of Cos7 cells for 40 h, the fluorescence intensity of both PI and HPF within the cytoplasm remained weak, and the cells remained alive. Furthermore, cell morphology showed large nuclei, abundant mitochondria, and subcellular organelles.

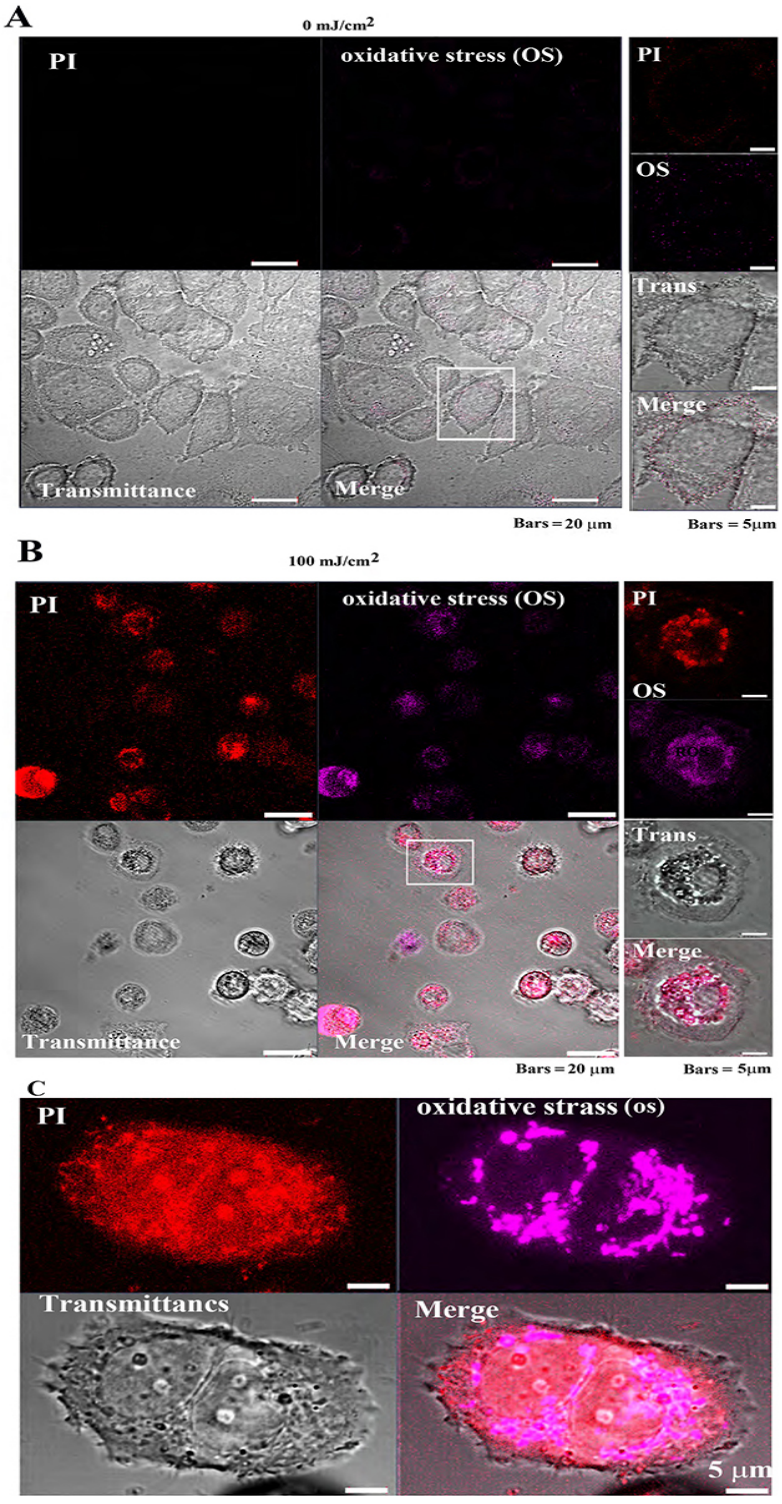

Fig. 7-1. Oxidative stress detection in MCF-7 cells following pulsed UV irradiation. (A) Control MCF-7 cell's (after 24 h of pulsed UV irradiation) PI and oxidative stress (OS) signal intensity are weakly distributed in the cytoplasm. (B) Twenty-four-hour UV-irradiated MCF-7 exhibited cell atrophy, cytoplasmic loss, and enriched nuclei. Most cells were PI-positive (cell death), and OS signals were also detected. Right panels: increased magnification of the white square in the left panel. (C) OS detection in a single MCF-7 cell. Observed images after 4 h of pulsed UV irradiation. Detection of OS in MCF-7 cells: Images were observed after 4 h of irradiation with pulsed UV at 100 mJ/cm^2. PI was widely localized in the cytoplasm, the nucleolus and OS were strongly luminescent, and OS was strongly luminescent, primarily in what appeared to be the mitochondria. The morphology was preserved, however, cells were PI-positive and considered dead. Bars = 5 μm. CellROX™ Deep Red Reagent was used to detect OS.

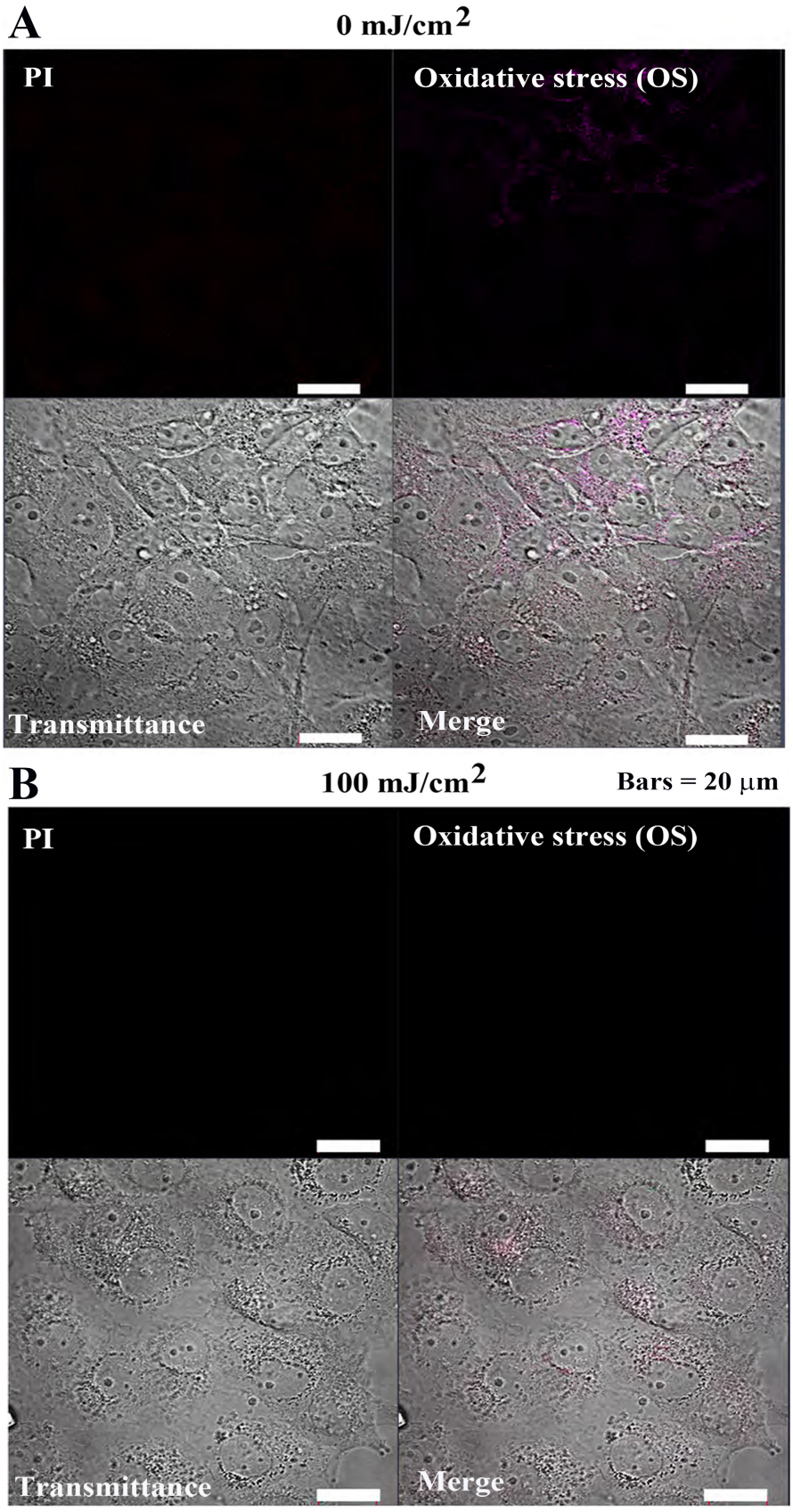

Fig. 7-2. Oxidative stress detection in Cos7 cells after 24 h of pulsed UV irradiation. (A) 0 mJ/cm^2 UV irradiation as control. (B)100 mJ/cm^2 UV irradiation. Cos7 cell PI and OS signal intensities were weakly distributed in the intracellular region. The cell structures were similar for the control and irradiated cells. Most cells were alive. CellROX™ Deep Red Reagent was used to detect OS.

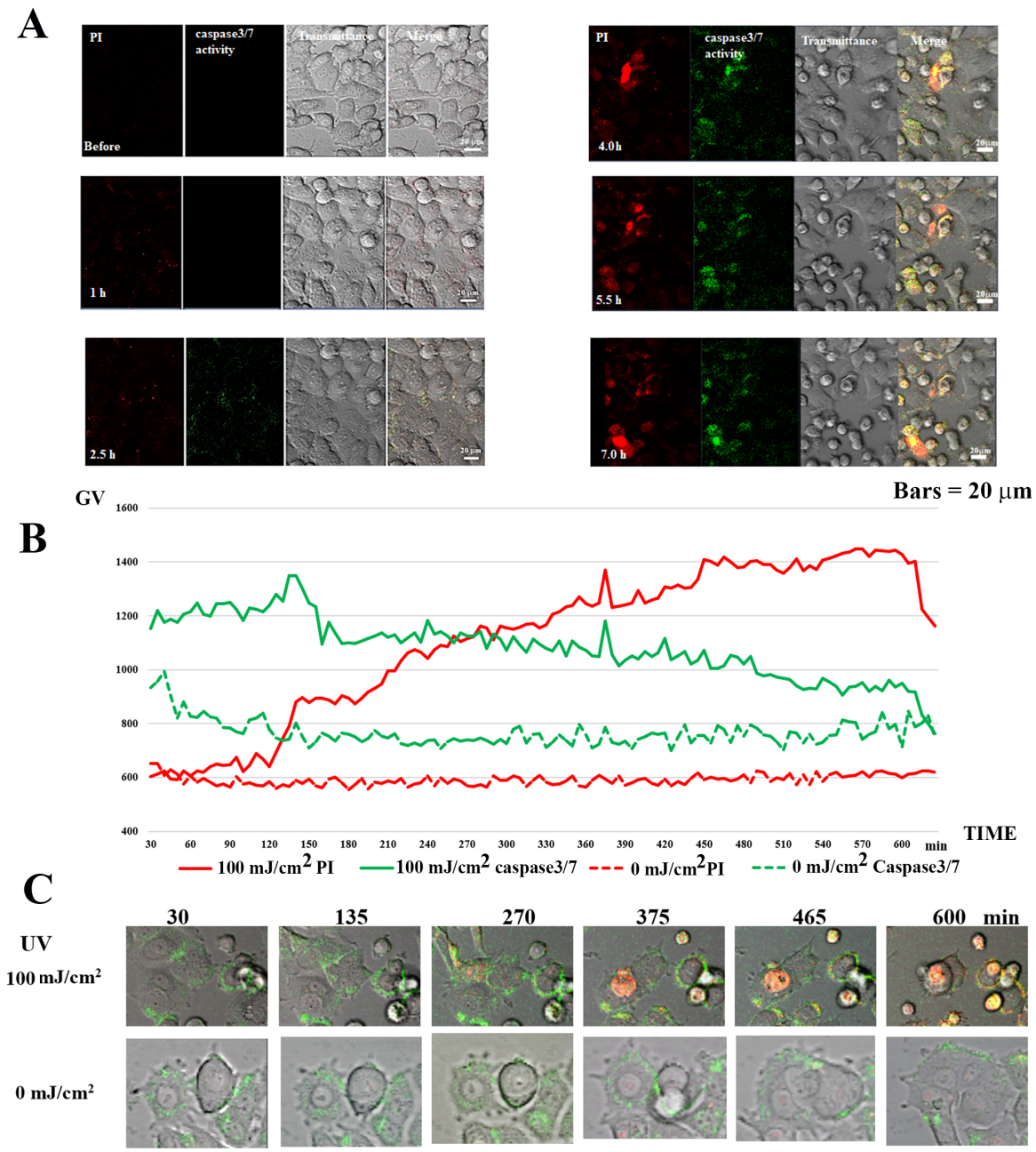

Fig. 8. Caspase 3/7 activity in UV-irradiated MCF-7 cells. (A) Caspase 3/7 and PI staining in 100 mJ/cm^2 UV irradiated MCF-7 cells; time-lapse observations were made before irradiation and at 1.0, 2.5, 4.5, and 7.0 h after irradiation. At 2.5 h post-irradiation, caspase 3/7 activity began to increase with time. PI was nuclear positive after 4 h. (B) Time lapse of Caspase 3/7 and PI staining of MCF-7 cells irradiated with 0 mJ/cm^2 and 100 mJ/cm^2 UV irradiation (X Axis: Time, Y Axis: Gray Value). (C) Caspase fluorescence luminance and PI fluorescence luminance at various time points. PI: red color, caspase: green color.

3.2.7 Hydroxyl Radical (•OH)

Observation of MCF-7 cells following UV irradiation for 24 h revealed that the control cells exhibited weak PI and •OH, fluorescence signals (Fig. 10A), while cells treated with 100 mJ/cm^2 UV irradiation exhibited relatively stronger signals for PI and •OH (Fig. 10B). Meanwhile, the cell morphology was unclear, with some cytoplasmic outflow and intracellular granules. However, given that the image was similar to the 100 mJ/cm^2 UV irradiation image in Fig. 3B, which were PI-positive, they were judged to be dead. In contrast, both the control and irradiated Cos7 cells exhibited weak PI and •OH fluorescence signals (Fig. 10B).

4. Discussion

Continuous UV-C irradiation has long been known to be effective in killing a wide range of bacterial species and

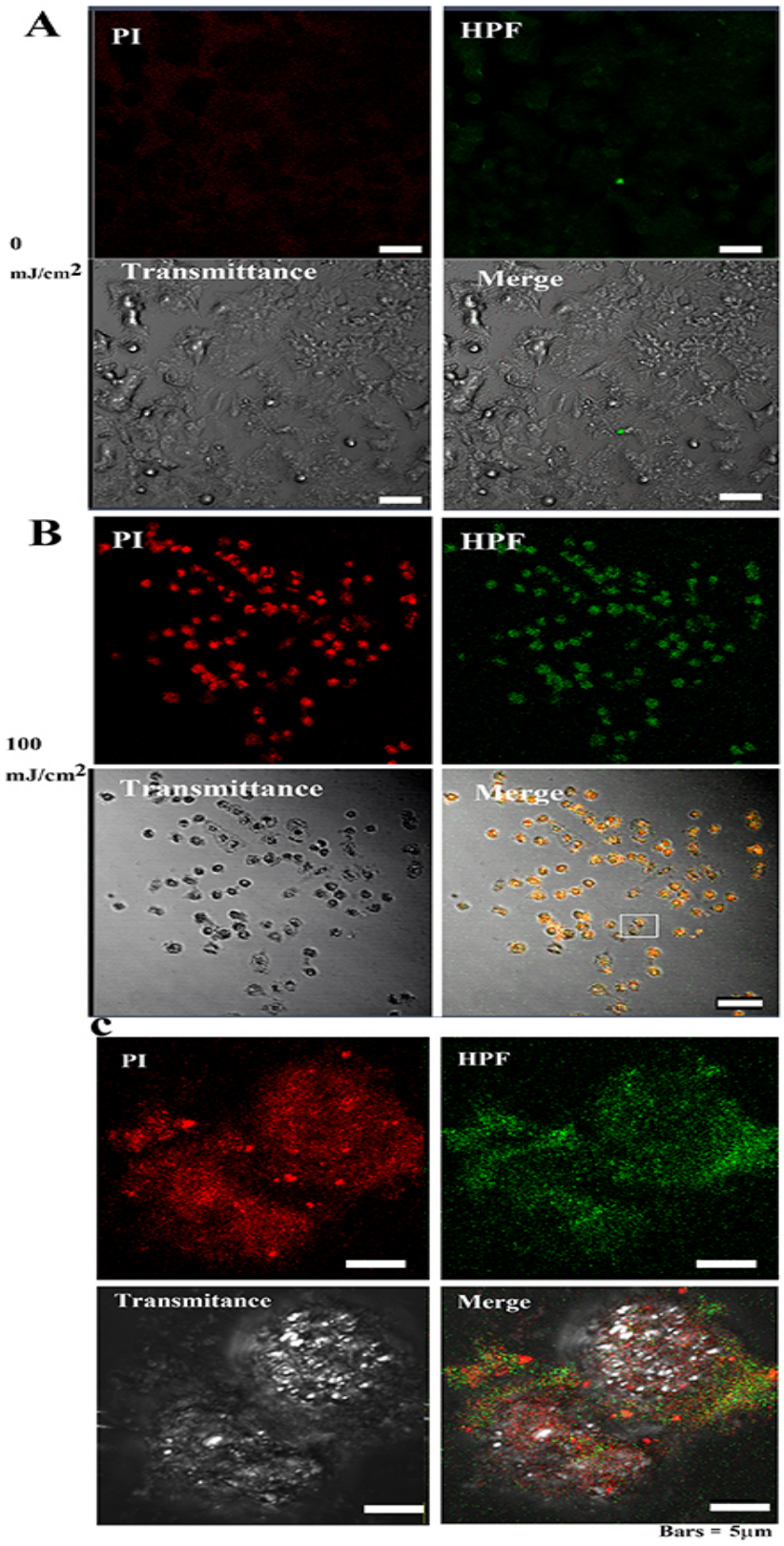

Fig. 9-1. •OH and 3-(p-hydroxyphenyl) fluorescein (HPF) abundance in MCF-7 cells after 40 hours of irradiation. (A) The PI and OS signal intensities in MCF-7 cells were weakly distributed in the cytoplasm of control cells. Bar = 50 μm. (B) Cell atrophy and cytoplasmic lysis were observed in irradiated cells. Most cells were PI- and HFP-positive (cell death) in the nuclei and cytoplasm. Nuclear enrichment was also observed. Bar = 50 μm. (C) High magnification of white squares appearing in (B); bar = 5 μm.

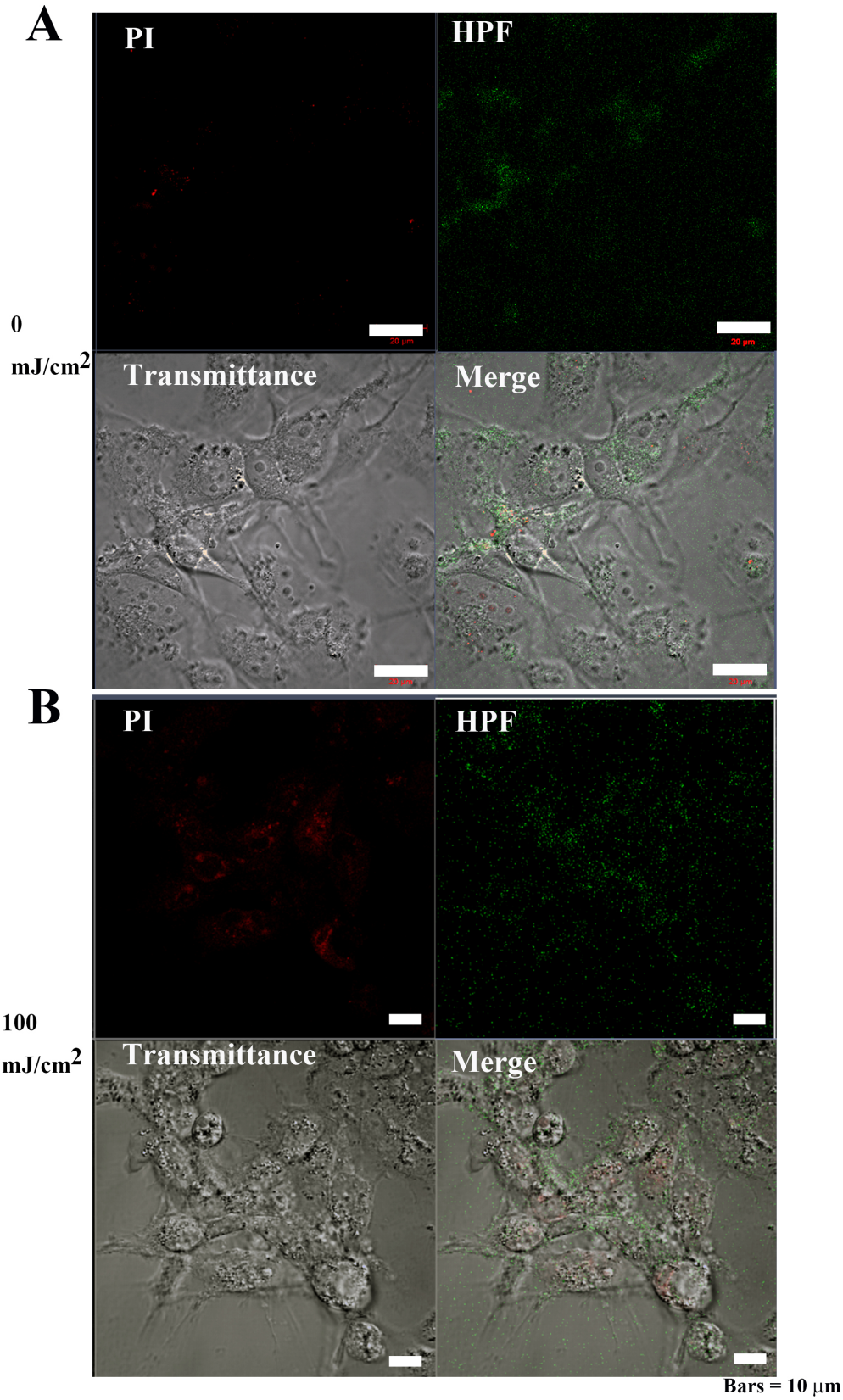

Fig. 9-2. OH and 3-(p-hydroxyphenyl) fluorescein (HPF) abundance in Cos7 cells after 40 hours of irradiation. (A) The signal intensities of PI and OS were weakly distributed in the cytoplasm of control Cos7 cells. Bar = 50 μm. (B) The signal intensities of PI and OS were weakly distributed in the cytoplasm of 100 mJ/cm^2 irradiated Cos7 cells at 50 μm. Normal cell structure was observed in the control and 100 mJ/cm^2 UV cells. Most cells were alive. Bars = 10 μm.

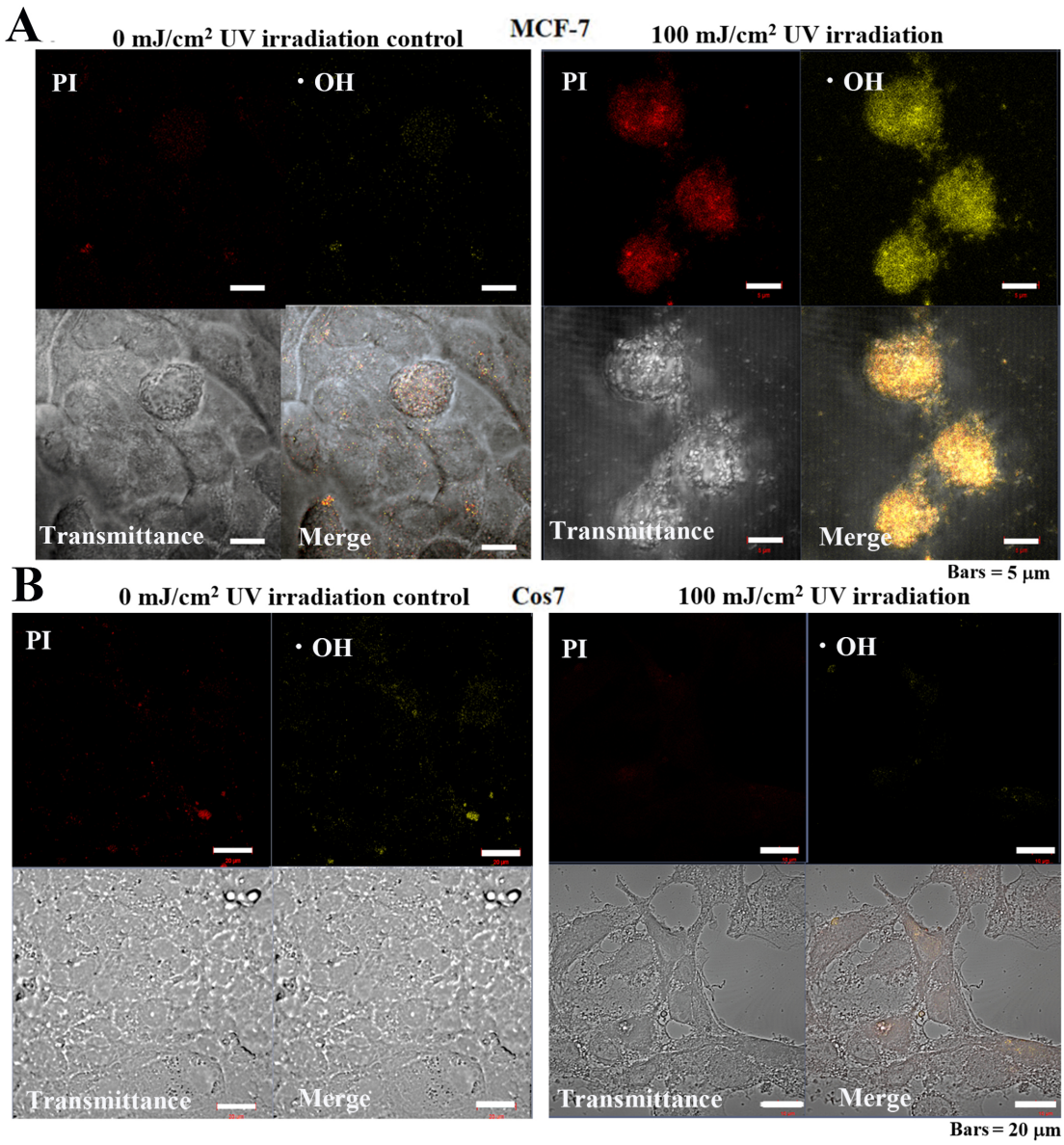

Fig. 10. Cellular mitochondrial ROS-OH580 activity under 24 h pulsed UV irradiation in MCF-7 and Cos7 cells. (A) The signal intensities of PI and ROS-OH580 in control MCF-7 cells were weakly distributed in the cytoplasm and nucleus. Bar = 5 μm. Cell atrophy and cytoplasmic lysis were observed in irradiated MCF-7 cells. Most cells were PI-positive (cell death), and the ROS-OH580 (•OH) signal was strongly detected in the nuclear enrichment. Bar = 5 μm. (B) PI and ROS-OH580 (•OH) signal intensities in Cos7 cells were weakly distributed in the cytoplasm of control and irradiated Cos7 cells. Bar = 5 μm.

has been used as a means of sterilization [22–24]. However, continuous irradiation with UV rays in such an environment requires a long irradiation time of 10–50 min. In recent years, pulsed UV light and food sterilization equipment have become increasingly popular. Pulsed UV sterilization can kill a wide range of bacteria, viruses, yeasts, and protozoa within a few seconds of irradiation [9–13].

In the current study, we attempted to apply a method of pulsed UV light, which has excellent bactericidal effects, for killing tumor cells. The pulsed UV irradiation method was demonstrated to be tumor effective when irradiated with 100 mJ/cm^2 against cancer cells such as human breast cancer cell lines. More specifically, tumor cells (MCF7, BT474), a human cervical cancer cell line (HeLa), human leukemia cell lines [MOLT/S, MOLT/TMQ 200 (trimethrexate anticancer drug-resistant 200 times), K562/Sl, 562/S2, K562/ARA-C (cytarabine anticancer drug-resistant)], human fibrous cell line (HT-1080), human prostate cancer cell lines (DU14, PC3), human choriocarcinoma malignant cell line (BeWo), and human kidney cancer cell lines (ACHN, Caki-1) demonstrated effects (data not shown). However, when non-tumor cells were irradiated with the same pulsed UV radiation energy as tumor cells, the non-tumor cells did not die but rather

survived. In fact, tumor cells were nearly completely killed by 100 mJ/cm^2 pulsed UV irradiation, whereas non-tumor cells survived (Fig. 2). Moreover, the selective killing of tumor cells did not occur with 100 mJ/cm^2 pulsed UV irradiation, excluding the UV-C region (Fig. 3). The integrated energy of pulsed UV that killed non-tumor cells was 3.24 J/cm^2. This phenomenon occurred at pulsed UV radiation energies of 3.24 J/cm^2 or less, to which cells were exposed, and cell activity increased at energies of 1 J/cm^2 or less.

Hence, we confirmed the phenomenon of selectively injuring and killing only tumor cells while negligible impacts on non-tumor cells (Table 1). Based on these findings, we proposed a new drug-free UV pulse irradiation cancer therapy method [PDT (PhotoDynamic Therapy) $\rightarrow$ pulsed photon therapy (PPT)], the proposed mechanism of this selective killing action is presented in Fig. 4.

4.1 Cellular Injury and Cell Death Hypothesis by Pulsed Ultraviolet Irradiation Membrane Disruption

The death receptors (Fas: CD95) on the cell membrane surface are expressed disproportionately by tumor cells compared to non-tumor cells [25–28]. Application of pulsed UV irradiation causes clustering of these death receptors, resulting in their trimerization and activation, similar to that following activation by a ligand [29]. Meanwhile, the pulsed light causes decarbonylation of the surface of living tissue cells, thereby improving light penetration into the body. However, pulsed light generates ROS and singlet oxygen only during pulsed irradiation [30].

Intracellularly, generation of ROS is induced, and •OH generation is promoted [31–33]. Subsequently, •OH causes protein denaturation, transport inhibition, and inactivation of essential cellular metabolic enzymes. Additionally, •OH acts on unsaturated fatty acids in the cell membrane. Collectively, this causes upregulation, denaturation, and destruction of membrane permeability.

4.2 Tumor Cells vs. Non-Tumor Cells

As mentioned above, tumor cells express higher levels of CD95 on their cell membrane compared to non-tumor cells. Upon pulsed UV irradiation, CD95 forms a cluster and undergoes trimerization, thereby stimulating the production of ROS. This phenomenon causes a domino-like chain reaction resulting in increased ROS production. However, the number of radical scavengers present in tumor cells is low, thus limiting the scavenging of ROS produced in the tumor cells, resulting in a further increase in ROS [34]. A subsequent chain reaction of ROS and •OH radical production proceeds, resulting in protein denaturation, transport inhibition, inactivation of essential metabolic enzymes, renewal, denaturation, and destruction of membrane permeability by radicals [16].

In contrast, given that non-tumor cells have fewer death receptors (CD95) [27], the presence of radical scavengers is high [34]. Hence, pulsed UV irradiation causes clustering of CD95 and activation of its trimer; however, ROS is produced in small quantities and readily scavenged, allowing the cells to return to their normal state without experiencing membrane destruction by OH radicals.

Our immunochemistry results support this hypothesis as CD95 localization was observed to be significantly greater in tumor cells versus non-tumor cells. More specifically, observations at the cellular level showed that the CD95 signals were localized at the plasma membrane surface (Fig. 5).

4.3 Apoptosis Analysis

Apoptosis is cell injury induced by continuous-wave light UV irradiation [20,21]. Moreover, for each cell, the effect of irradiation with a UV pulse flash at a prescribed frequency in the same manner as described above for early-stage apoptosis (DNA disorder) was studied. Using Annexin V as a marker, early-stage apoptosis was analyzed by CLSM. At an early stage of apoptosis, PS, found inside the cell membrane, is expressed on the outside, where it binds with Annexin V. Annexin V is a protein of 35–36 kDa that bonds with phospholipid in a Ca^{2+}-dependent manner. The expression of PS outside the cell membrane is followed by loss of a normal cell membrane structure and initiation of DNA fragmentation or chromatin agglomeration. Based on this principle, by detecting binding with Annexin V, an early-stage apoptotic cell is recognized. However, in the current study, following irradiation of cells for 24 h, weak Annexin V signals were detected in MCF-7 and Cos7 cells. Thus, the molecular mechanism underlying the targeted killing effect of pulsed UV light irradiation does not likely rely significantly on apoptosis, which agrees with previously published studies [35,36].

4.4 Detection of Oxidative Stress in Tumor and Non-Tumor Cells

Tumor cells irradiated with 0 mJ/cm^2 UV were negative for both OS and PI, and their morphology was normal. However, cells exposed to UV irradiation (100 mJ/cm^2) were positive for both OS and PI. The morphology of these cells included atrophy, cytoplasmic lysis, and membrane blurring. The cells were observed to be dead. In fact, by 4 h after irradiation, the entire cytoplasm was PI-positive, OS was positive in the area anticipated to be the mitochondria; the morphology showed cell atrophy, cytoplasmic lysis, membrane blurring, and the nucleus structure was still maintained, suggesting that the cells were dead. Hence, pulsed UV irradiation induces OS. In contrast, in non-tumor cells, both PI and OS signals were weak after 0 mJ/cm^2 or 100 mJ/cm^2 UV irradiation. No differences in cell morphology were observed between the tumor and non-tumor cells (Figs. 7-1,7-2).

4.5 Caspase-3/7 Activity in Tumor and Non-Tumor Cells

Time-lapse observation of pulsed UV irradiation at 100 mJ/cm^2 showed that caspase-3/7 fluorescence intensity increased 30 min after irradiation, while PI fluorescence intensity did not change. This indicated that caspase-3/7 was activated at 30 min. At 2.5 h post-irradiation, caspase-3/7 fluorescence intensity peaked and then decreased, indicating that the PI fluorescence intensity increased rapidly and that the cell membrane was beginning to weaken, leading to cell death. One portion of the cells was lost due to cell rupture at 7 h post-irradiation. However, at 0 mJ/cm^2 UV irradiation, caspase-3/7, and PI fluorescence intensity remained unchanged at a low level. Hence, pulsed UV irradiation activated caspase-3/7 in the cytoplasm, and after cell death, it decreased and disappeared as soon as the cells were destroyed (Fig. 8).

4.6 Detection of Reactive Oxygen Species (ROS) in Tumor and Non-Tumor Cells

When the oxidative damaging power of ROS and free radicals generated in the body outweighs the antioxidant power (radical scavengers) in the body, oxidative stress rises and leads to the production of OH radicals [37,38].

In control tumor cells exposed to 0 mJ/cm^2 UV irradiation, only weak fluorescence intensity was observed for both PI and HPF, and the cells were viable. Meanwhile, at 100 mJ/cm^2 UV irradiation, PI staining was observed primarily in the nucleus, while that of HPF was in the cytoplasm. More specifically, the PI fluorescence surrounded the condensed nuclear-like structures. TEM images further showed condensed nuclei-like structures and areas surrounding obscured cytoplasm.

In contrast, within control non-tumor cells, HPF fluorescence was observed in some cells, and cell morphology was normal, while for the irradiated cells, weak PI and HPF fluorescence were observed in the cytoplasm. Taken together, these findings indicate that pulsed UV irradiation showed strong HPF fluorescence intensity in tumor cells and negligible fluorescence intensity in non-tumor cells (Figs. 9-1,9-2).

4.7 Hydroxyl Radical (•OH) Tumor and Non-Tumor Cells

In control tumor cells, negligible levels of UV PI or •OH fluorescent signals were detected. Alternatively, in irradiated tumor cells, strong fluorescent signals were detected in the nuclei for both PI and •OH. Meanwhile, in non-tumor cells, no PI nor •OH fluorescent signals were observed in the control or irradiated cells (Fig. 10).

In tumor cells, the intracellular chain reaction of radical production induced by UV irradiation seems to exceed the scavenging function, leading to cell death. In contrast, in non-tumor cells, although UV-induced intracellular radical reactions occurred, the radical scavenging function was superior, suggesting that the cells underwent repair and survived [32,39–42]. However, when the same energy irradiation was performed with a continuous UV mercury lamp, both tumor and non-tumor cells were killed, and the phenomenon of selective tumor cell death did not occur (data not shown). Hence, as hypothesized, the observed phenomenon only occurred with pulsed UV irradiation.

5. Conclusions

The current method shows that tumor cells are selectively killed at a range value by different irradiation doses of pulsed UV light. Hence, only tumor cells can be selectively killed. Without the need for drug injection pretreatment (drug-free), only tumor cells can be easily eliminated in a short time without causing cell death of non-tumor cells simply via irradiation with pulsed ultraviolet light. It is believed that this strategy can be applied to identify drug-free treatments for tumor cancer tissues. In particular, we hope to use this principle to develop endoscopic treatment, intraoral treatment, and body-surface tumor irradiation devices. Collectively, this study suggests that the application of PDT (PhotoDynamic Therapy) to PPT (Pulsed Photon Therapy) is possible and effective.

Abbreviations

PDT, PhotoDynamic Therapy; PPT, Pulsed photon therapy; UV, Ultraviolet; ROS, reactive oxygen species; NIR-PIT, near-infrared photoimmunotherapy; SUPR, super-enhanced permeability and retention effects; DMEM, Dulbecco's modified Eagle's medium; PFA, paraformaldehyde; PI, propidium iodide; TEM, transmission electron microscope; SEM, scanning electron microscope; PBS, phosphate-buffered saline; EDTA, ethylenediaminetetraacetic acid; BSA, bovine serum albumin; TMRE, tetramethylrhodamine ethyl ester; DEVD, a four-amino acid peptide; HPF, 3,3-(p-Hydroxyphenyl) fluorescein; DMF, imethylformamide; CLSM, Confocal Laser Scanning Microscopy; PS, phosphatidylserine; •OH, hydroxyl radical; OS, oxidative stress; TMQ, trimethrexate.

Author Contributions

JI and YI performed the experiments and analyzed the data. JI designed the study and wrote the manuscript. All authors contributed to editorial changes in the manuscript. All authors read and approved the final manuscript.

Ethics Approval and Consent to Participate

Not applicable.

Acknowledgment

We thank Thunderlight Corporation for providing the S-BP60 ultraviolet light irradiation system. This study was conducted using facilities of the Tokai University School of Medicine Office.

Funding

This research received no external funding.

Conflict of Interest

The authors declare no conflict of interest.

References

[1] Mitsunaga M, Ogawa M, Kosaka N, Rosenblum LT, Choyke PL, Kobayashi H. Cancer cell–selective in vivo near infrared photoimmunotherapy targeting specific membrane molecules. Nature Medicine. 2011; 17: 1685–1691.

[2] Kobayashi H, Watanabe R, Choyke PL. Improving Conventional Enhanced Permeability and Retention (EPR) Effects; what is the Appropriate Target? Theranostics. 2014; 4: 81–89.

[3] Tanaka M, Mroz P, Dai T, Huang L, Morimoto Y, Kinoshita M, *et al*. Photodynamic therapy can induce a protective innate immune response against murine bacterial arthritis via neutrophil accumulation. PLoS ONE. 2012; 7: e39823.

[4] Kobayashi H, Choyke PL. Super enhanced permeability and retention (SUPR) effects in tumors following near infrared photoimmunotherapy. Nanoscale. 2016; 8: 12504–12509.

[5] Takada A, Matsushita K, Horioka S, Furuichi Y, Sumi Y. Bactericidal effects of 310 nm ultraviolet light-emitting diode irradiation

[6] Narita K, Asano K, Morimoto Y, Igarashi T, Hamblin MR, Dai T, *et al*. Disinfection and healing effects of 222-nm UVC light on methicillin-resistant Staphylococcus aureus infection in mouse wounds. Journal of Photochemistry and Photobiology B. 2018; 178: 10–18.

[7] Ko G, First MW, Burge HA. Influence of relative humidity on particle size and UV sensitivity of Serratia marcescens and Mycobacterium bovis BCG aerosols. Tubercle and Lung Disease. 2000; 80: 217–228.

[8] Bak J, Begovic T. A prototype catheter designed for ultraviolet C disinfection. The Journal of Hospital Infection. 2013; 84: 173–177.

[9] Krishnamurthy K, Demirci A, Irudayaraj J. Inactivation of Staphylococcus aureus by Pulsed UV-Light Sterilization. Journal of Food Protection. 2004; 67: 1027–1030.

[10] Umezawa K, Asai S, Inokuchi S, Miyachi H. A Comparative Study of the Bactericidal Activity and Daily Disinfection Housekeeping Surfaces by a New Portable Pulsed UV Radiation Device. Current Microbiology. 2012; 64: 581–587.

[11] Abe H, Shiba M, Niibe Y, Tadokoro K, Satake M. Pulsed xenon flash treatment inactivates bacteria in apheresis platelet concentrates while preserving *in vitro* quality and functionality. Transfusion. 2017; 57: 989–996.

[12] Abe H, Endo K, Shiba M, Niibe Y, Miyata S, Satake M. Flow path system of ultraviolet C irradiation from xenon flash to reduce bacteria survival in platelet products containing a platelet additive solution. Transfusion. 2020; 60: 1050–1059.

[13] Bhavya ML, Umesh Hebbar H. Pulsed light processing of foods for microbial safety. Food Quality and Safety. 2017; 1: 187–202.

[14] Fine F, Gervais P. Efficiency of pulsed UV light for microbial decontamination of food powders. Journal of Food Protection. 2004; 67: 787–792.

[15] Le Gallo M, Poissonnier A, Blanco P, Legembre P. CD95/Fas, Non-Apoptotic Signaling Pathways, and Kinases. Frontiers in Immunology. 2017; 8: 1216.

[16] Yamamoto R, Shimamoto K, Ishii Y, Kimura M, Fujii Y, Morita R, *et al*. Involvement of PTEN/Akt signaling and oxidative stress on indole-3-carbinol (i3C)-induced hepatocarcinogenesis in rats. Experimental and Toxicologic Pathology. 2013; 65: 845–852.

[17] Levoin N, Jean M, Legembre P. CD95 Structure, Aggregation and Cell Signaling. Frontiers in Cell and Developmental Biology. 2020; 8: 314.

[18] Declercq W, Vanden Berghe T, Vandenabeele P. RIP Kinases at the Crossroads of Cell Death and Survival. Cell. 2009; 138: 229–232.

[19] Scaffidi C, Fulda S, Srinivasan A, Friesen C, Li F, Tomaselli KJ, *et al*. Two CD95 (APO-1/Fas) signaling pathways. The EMBO Journal. 1998; 17: 1675–1687.

[20] Omoteyama K, Inoue S, Salah-eldin A. Cell growth inhibition and apoptosis in cancer cells. Cytometry Research. 2002; 12: 83–91.

[21] Sun X, Ai M, Wang Y, Shen S, Gu Y, Jin Y, *et al*. Selective Induction of Tumor Cell Apoptosis by a Novel P450-mediated Reactive Oxygen Species (ROS) Inducer Methyl 3-(4-Nitrophenyl) Propiolate. Journal of Biological Chemistry. 2013; 288: 8826–8837.

[22] Schiller M, Bekeredjian-Ding I, Heyder P, Blank N, Ho AD, Lorenz HM. Autoantigens are translocated into small apoptotic bodies during early stages of apoptosis. Cell Death and Differentiation. 2008; 15: 183–191.

[23] Andersen BM, Bånrud H, Bøe E, Bjordal O, Drangsholt F. Comparison of UV C Light and Chemicals for Disinfection of Surfaces in Hospital Isolation Units. Infection Control & Hospital Epidemiology. 2006; 27: 729–734.

[24] Carling PC, Von Beheren S, Kim P, Woods C. Intensive care unit environmental cleaning: an evaluation in sixteen hospitals using a novel assessment tool. Journal of Hospital Infection. 2008; 68: 39–44.

[25] Kulms D, Zeise E, Pöppelmann B, Schwarz T. DNA damage, death receptor activation and reactive oxygen species contribute to ultraviolet radiation-induced apoptosis in an essential and independent way. Oncogene. 2002; 21: 5844–5851.

[26] Bębenek M, Duś D, Kożlak J. Prognostic value of the Fas/Fas ligand system in breast cancer. Contemporary Oncology. 2013; 17: 120–122.

[27] Peter ME, Hadji A, Murmann AE, Brockway S, Putzbach W, Pattanayak A, *et al*. The role of CD95 and CD95 ligand in cancer. Cell Death & Differentiation. 2015; 22: 549–559.

[28] Fouqué A, Legembre P. The CD95/CD95L Signaling Pathway: A Role in Carcinogenesis. Cancer Immunology. 2020; 26: 171–188.

[29] Rehemtulla A, Hamilton CA, Chinnaiyan AM, Dixit VM. Ultraviolet Radiation-induced Apoptosis is Mediated by Activation of CD-95 (Fas/APO-1). Journal of Biological Chemistry. 1997; 272: 25783–25786.

[30] Bell AF, Stoner-Ma D, Wachter RM, Tonge PJ. Light-Driven Decarboxylation of Wild-Type Green Fluorescent Protein. Journal of the American Chemical Society. 2003; 125: 6919–6926.

[31] Jeong EM, Yoon J, Lim J, Shin J, Cho AY, Heo J, *et al*. Real-Time Monitoring of Glutathione in Living Cells Reveals that High Glutathione Levels are Required to Maintain Stem Cell Function. Stem Cell Reports. 2018; 10: 600–614.

[32] Georgieva E, Zhelev Z, Aoki I, Bakalova R, Higashi T. Detection of Redox Imbalance in Normal Lymphocytes with Induced Mitochondrial Dysfunction – EPR Study. Anticancer Research. 2016; 36: 5273–5280.

[33] Cohn CA, Simon SR, Schoonen MA. Comparison of fluorescence-based techniques for the quantification of particle-induced hydroxyl radicals. Particle and Fibre Toxicology. 2008; 5: 2.

[34] Kopustinskiene DM, Jakstas V, Savickas A, Bernatoniene J. Flavonoids as Anticancer Agents. Nutrients. 2020; 12: 457.

[35] Nocentini S. Apoptotic response of malignant rhabdoid tumor cells. Cancer Cell International. 2003; 3: 11.

[36] Tait SWG, Ichim G, Green DR. Die another way – non-apoptotic

mechanisms of cell death. Journal of Cell Science. 2014; 127: 2135–2144.
[37] Oberley LW, McCormick ML, Sierra-Rivera E, Kasemset-St Clair D. Manganese superoxide dismutase in normal and transformed human embryonic lung fibroblasts. Free Radical Biology and Medicine. 1989; 6: 379–384.
[38] Isoherranen K, Peltola V, Laurikainen L, Punnonen J, Laihia J, Ahotupa M, *et al*. Regulation of copper/zinc and manganese superoxide dismutase by UVB irradiation, oxidative stress and cytokines. Journal of Photochemistry and Photobiology B: Biology. 1997; 40: 288–293.
[39] Dhar SK, St. Clair DK. Manganese superoxide dismutase regulation and cancer. Free Radical Biology and Medicine. 2012; 52: 2209–2222.
[40] Chaiswing L, Zhong W, Oberley TD. Increasing discordant antioxidant protein levels and enzymatic activities contribute to increasing redox imbalance observed during human prostate cancer progression. Free Radical Biology and Medicine. 2014; 67: 342–352.
[41] Pan J, He H, Su Y, Zheng G, Wu J, Liu S, *et al*. GST-TAT-SOD: Cell Permeable Bifunctional Antioxidant Enzyme—a Potential Selective Radioprotector. Oxidative Medicine and Cellular Longevity. 2016; 2016: 5935080.
[42] Haider K, Haider MR, Neha K, Yar MS. Free radical scavengers: an overview on heterocyclic advances and medicinal prospects. European Journal of Medicinal Chemistry. 2020; 204: 112607.